International Journal of Impact Engineering 136 (2020) 103427

Contents lists available at ScienceDirect

International Journal of Impact Engineering

journal homepage: www.elsevier.com/locate/ijimpeng

Target penetration and impact analysis of intermetallic projectiles

Colton Cagle[a], Kevin J. Hill[a], Connor Woodruff[a], Michelle L. Pantoya[a,*], Joseph Abraham[b], Casey Meakin[b,c]

[a] Texas Tech University, Mechanical Engineering Department, Lubbock, TX 79409 USA
[b] Karagozian and Case, Inc.,700N Brand Blvd, Suite 700, Glendale, CA 91203 USA
[c] Meakin Technologies, Pasadena, CA 91104 USA

ARTICLE INFO

Keywords:
Penetration
Fragmentation
Intermetallic projectile
Flame spread
Plastic deformation

ABSTRACT

A High-velocity Impact-ignition Testing System (HITS) was developed to study the dynamic response of intermetallic projectiles penetrating through two aluminum plates at impact velocities up to 1300 m/s. The intermetallic projectiles are contained in a 0.410 caliber shot gun shell and launched from a propellant driven gun into a catch chamber equipped with view ports and imaging diagnostics. Penetration, impact, and reaction are monitored using high-speed cameras that provide macroscopic and localized perspectives of projectile and target interaction. Several key results include the following. The first-plate penetration of the projectile follows well established ballistic curve fits. Subsequent plate penetration shows significant deviations attributed to projectile damage resulting from the first plate impact. The damage imparted to the projectile transitions from significant plastic deformation to severe fragmentation as impact velocity increases. Penetration of the aluminum target plate is significantly affected by the fragmentation field and show a 45% increase in rupture size at the highest impact velocity case. Combustion within the fragmented projectile is observed starting at 850 m/s. These results show the transition in dynamic interaction between multiple target plates at increasing projectile impact velocity.

1. Introduction

Intermetallic composites consist of two or more metallic elements that are combined in order to exploit their mechanical, chemical, electrical or physical properties toward an application. Some examples of intermetallic reactions include shape memory alloys, corrosion and microbial resistant coatings, or high temperature structural materials. Varma [1] presents an overview of various intermetallic reactions and the properties that make the product alloys useful for various applications. From a chemical perspective, intermetallic reactions are interesting to study because they undergo various stages of reaction such as phase change and reactive sintering, followed by reactions dependent upon metalloid or alloy phase, as well as oxidation reactions with the surrounding environment [2]. Most stages of reaction are exothermic and offer the potential to harness chemical energy for localized heating.

Intermetallic projectiles can increase energy deposition into a target through exothermic reactions triggered by fragmentation from the penetration or impact event. Many studies that have examined intermetallic projectiles use high density metals such as aluminum (Al) and tungsten (W) [3–7]. Previous research laid the foundation for understanding that monitoring quasi-static pressure upon penetration and reaction provides little insight into energy deposition because intermetallic reactions are generally not gas generating, so pressure variations are minimal. This study extends previous work on impact experiments with intermetallic projectiles that measured transient pressure [3–7] by providing new data from high speed videography of intermetallic projectile penetration and impact events. The objective is to examine the effect of projectile velocity on penetration, fragmentation and reaction through two aluminum plates followed by impact onto a steel anvil. This objective is accomplished using multiple high-speed cameras and focusing lenses to capture macroscopic and localized perspectives of projectile and target interaction as well as analyzing the penetrated plates for their deformation characteristics.

2. Experimental

The High-velocity Impact-ignition Testing System (HITS) is schematically shown in Fig. 1 and detailed in Hill et al. [8] but summarized here. The entire apparatus measures 2.44 m in length by 0.92 m in width for a total of 2.23 m^2 of occupied floor space making this setup

* Corresponding author.
E-mail address: michelle.pantoya@ttu.edu (M.L. Pantoya).

https://doi.org/10.1016/j.ijimpeng.2019.103427
Received 26 June 2019; Received in revised form 23 October 2019; Accepted 24 October 2019
Available online 25 October 2019

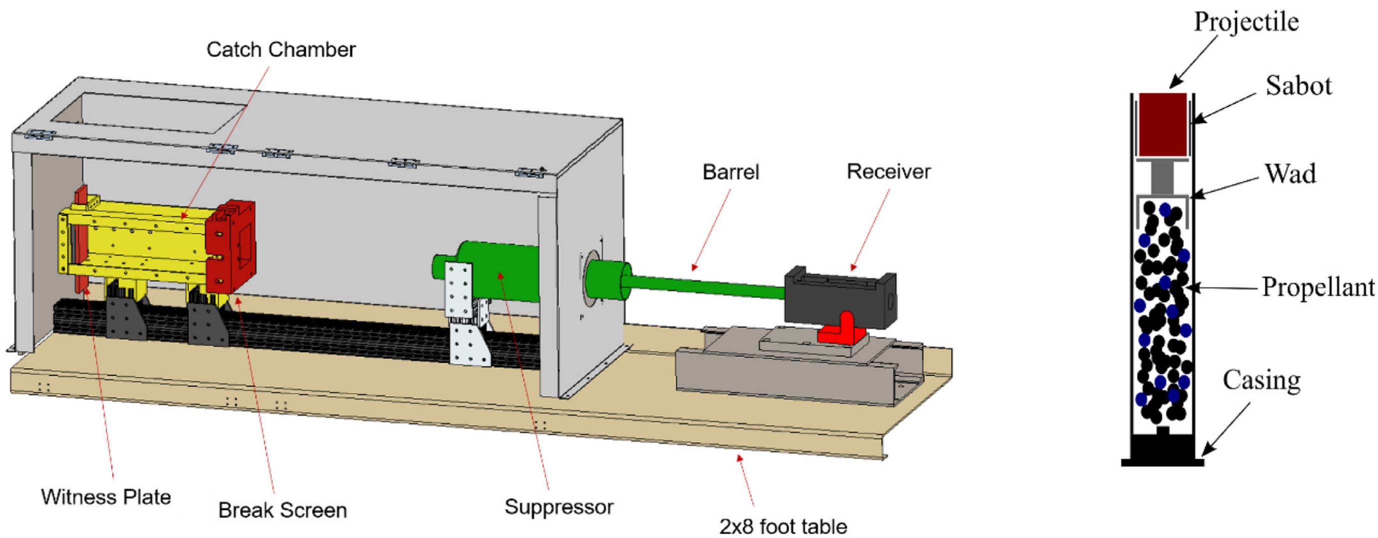

Fig. 1. (Left) Schematic of HITS apparatus showing the receiver and barrel coupled with a suppressor that is housed in a cabinet that also includes the catch chamber with a view port, break screen, pressure sensors, and steel anvil witness plate. (Right) Schematic of the loaded 0.410 casing assembly showing projectile, sabot, wad, and propellant.

smaller than most conventional high velocity impact systems. A 0.410 caliber shot gun is used to launch projectiles into an instrumented catch chamber (see Fig. 1). The projectiles travel 60 cm from the barrel to penetrate through two 0.32 cm thick 6061-T6 aluminum plates before impacting a modular, hardened steel anvil. Tests are designed to allow penetration through two plates separated by 10 cm. A 10 cm separation distance is selected to allow suitable visualization of the impact, fragmentation, and reaction events through each portion of the chamber.

The intermetallic projectile is a cylindrical pellet with 1 cm diameter by 1 cm length and 3.05 g of binary metallic powder composed of aluminum and zirconium that is pressed to a consolidated volume of 0.6787 cm^3 giving a total density of 4.49 g/cm^3. The projectile is inserted into a nylon sabot and loaded into a 0.410 primed shotgun shell filled with Blue Dot shotgun propellant (made by Alliant Powder®). A wad with the shot cup removed is inserted between the projectile and the propellant to assist in gas sealing within the barrel. The projectile velocity is linearly proportional to the amount of Blue Dot propellant. Three different masses of propellant: 800 mg, 1350 mg, and 2300 mg are used to achieve three different impact velocities: 500 m/s, 850 m/s, and 1300 m/s, respectively. The impact velocities 500 m/s, 850 m/s, and 1300 m/s are selected because they each induce different projectile-target interactions during penetration and impact. It is noted that other impact velocities were tested, although they were ultimately redundant for discussion and not included here.

The assembled shell is loaded into the receiver of the HITS (Fig. 1) and the shell is fired. The projectile passes through a break screen composed of thin paper sandwiched between perforated aluminum foil (biased with a 9 V battery) to trigger the cameras. A minimum of three tests are performed for each impact velocity.

Experimental data are visual. The post-penetration perforated plates are analyzed from various perspectives with photographs. The *in-situ* projectile and target interactions are captured using two high-speed cameras: (1) Phantom v710 color camera, and (2) Phantom v2512 monochrome camera, that record both a macroscopic view of the entire catch chamber (at 49,000 fps) and a more localized, detailed view of plate penetration (at 460,000 fps), respectively. The cameras are positioned perpendicular to the direction of projectile motion and aligned with a side viewing window in the catch chamber (not shown in Fig. 1). The window is made of 1.5 cm polycarbonate to prevent blowout. A white sheet of paper is placed along the back of the chamber to improve projectile visualization and flame tracking during post processing of the video data. The high-speed cameras enable qualitative measurements of fragmentation and flame spreading as well as quantify impact velocity.

3. Results and discussion

3.1. Impact velocity

The projectile velocities from before and after each penetration event are defined as the impact and residual velocities, respectively. Table 1 summarizes the projectile impact and residual velocities for each target plate and the velocity reduction caused by penetration. For example, the first plate has an impact velocity of 481 m/s with a residual velocity of 396 m/s, and therefore a velocity reduction of 85 m/s. First plate experiments show a standard deviation in impact and residual velocity measurements within 6%. Second plate velocity standard deviation increases to 15%, and steel anvil impact velocity standard deviation increases to 20%. The standard deviations may be attributed to small degrees of projectile obliquity upon impact that is random between experiments. Also, there is likely a cascading effect between first and second plate velocities that contribute towards the standard deviations between experiments. For example, there is an increased velocity reduction caused by the second plate penetration, and as the projectile impact velocity increases, the percent velocity reduction decreases. The data in Table 1 is further plotted in Fig. 2.

Table 1
Impact and residual velocity and percent velocity reduction for various measurement locations throughout the test chamber for low, medium, and high impact velocity cases. The percentage velocity reduction is measured as the percentage reduction between the first and second plate velocities and the second plate and steel anvil velocities.

Impact Target Sequence	Impact Velocity (*m/s*)	Residual Velocity (*m/s*)	Velocity Reduction (*m/s*)	Percent Velocity Reduction
First plate	481	396	85	18%
Second plate	396	121	275	69%
Steel Anvil	121	–	–	–
First plate	850	693	157	18%
Second plate	693	352	341	49%
Steel Anvil	352	–	–	–
First plate	1300	1161	139	11%
Second plate	1161	760	371	35%
Steel Anvil	760	–	–	–

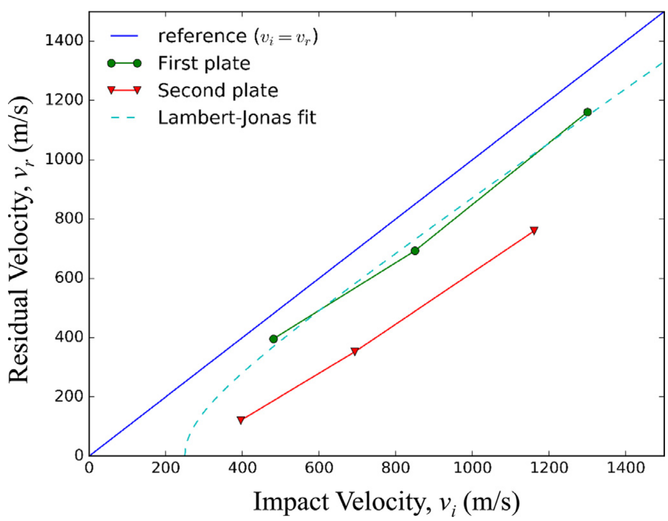

Fig. 2. Ballistic curves for experimental data showing projectile residual velocity as a function of impact velocity for first and second plate impacts.

Fig. 2 shows ballistic curves and the relationship between the residual and impact velocity. The data in Table 1 are separated into first plate and second plate impacts curves in Fig. 2. In both cases, the ballistic curves in Fig. 2 show relatively linear trends with slopes of approximately unity which is typical for penetrators with velocities sufficiently above the minimum velocity for which perforation is expected, also known as the ballistic limit velocity.

The linear trend in residual velocity in Fig. 2 for the first plate penetration follows similar linear trends seen in the literature and can be well fitted by the empirical relationship by Lambert and Jonas [9] in Eq. (1).

$$v_r = a(v_i^p - v_{BL}^p)^{1/p} \tag{1}$$

The residual velocity is v_r and the impact velocity is v_i. The fitting coefficients ($a \sim 0.9$, $p \sim 2.0$, $v_{BL} \sim 250\,m/s$) are based on a least-squares fit to cylindrical steel projectiles penetrating thin steel plates over a velocity range similar to the experiments presented by Elek et al. [10].

In determining the relationships between the impact and residual velocities, the 500 m/s case provides the most insight because the projectile from the 500 m/s impact velocity does not fragment after penetration through the first or second plates. Because the projectile stays intact upon penetrating the first plate, the second plate penetration analysis is treated similarly to the first plate penetration analysis and it is assumed that the impact velocity for the second plate follows the Lambert-Jonas [9] fit. However, in Fig. 2 the second plate linear trend does not follow the Lambert-Jonas [9] fit because the residual velocity for the 500 m/s impact is much lower than predicted. There are several possible explanations for the deviation between model and experiments for the second plate.

First, the deformation of the projectile due to the first plate impact might affect the penetration mechanics of the model. Fig. 3 shows plastic deformation that the projectile undergoes in the form of mushrooming after penetration of the first plate. For the 500 m/s impact velocity case the deformed projectile expands in diameter by 24%. Projectile plastic deformation is not seen at impact velocities higher than 500 m/s because the projectile fragments at velocities higher than 500 m/s. A fragmented or deformed projectile cannot be modelled with the same penetration mechanics as a cylindrical projectile. Woodward [11] describes the process in which a flat cylindrical projectile penetrates a target and cylindrically symmetrical shear bands are pushed in front of the projectile. These shear bands then meet at the back of the target plate and allow slip to occur along the shear bands more readily. When mushrooming occurs in the projectile, symmetrical shear bands

Fig. 3. Photograph of mushroomed projectile recovered from impact velocity of 500 m/s. Left side retained the original diameter of the projectile: 1 cm diameter. The mushroomed portion expanded in diameter by 24%: 1.24 cm. Impact velocities greater than 500 m/s resulted in fragmented projectiles upon penetration of the first target plate.

cannot form as readily, resulting in asymmetrical shear banding, and increasing the apparent strength of the aluminium plates.

Second, the penetration mechanics of aluminum plates are a complex function of the strain rate during impact. Models from Gilat et al. [12] predict that the magnitude of effective shear stress during penetration increases exponentially as a function of strain rate ($\dot{\epsilon}$). Strain rate is calculated in Eq. (2) by dividing the average penetration velocity (v_{perf}) by the thickness of the target plate (t_p). The penetration velocity is the average of the impact and residual velocity before and after penetration of each plate.

$$\dot{\epsilon} = \frac{v_{perf}}{t_p} \tag{2}$$

Using the Gilat models [12], the estimated effective shear stress for each penetration event is shown in Table 2. The magnitudes of all calculated strain rates are within $10^5\ sec^{-1}$, and according to the model, the exponential relationship between shear stress and strain rate begins at $10^4\ sec^{-1}$. The effective shear stress more than doubles from the 500 to 1300 m/s velocities, indicating that small changes in strain rate are subject to notable increases in effective shear stress.

Fig. 4 shows a representative graph illustrating the relationship between the Gilat models [12] for effective shear stress and velocity

Table 2
Strain rates and effective shear stress in aluminum target plates for all impact velocities from analysis using Gilat models [12].

Impact Velocity (m/s)	First Plate Strain Rate (sec^{-1})	Second Plate Strain Rate (sec^{-1})	First Plate Effective Shear Stress (GPa)	Second Plate Effective Shear Stress (GPa)
500	$1.4*10^5$	$0.8*10^5$	0.35	0.33
850	$2.4*10^5$	$1.6*10^5$	0.42	0.39
1300	$3.9*10^5$	$3.0*10^5$	0.75	0.49

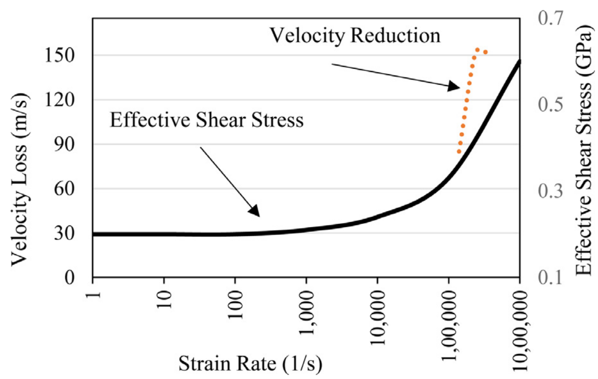

Fig. 4. Effective shear stress and velocity reduction as a function of strain rate. The velocity reduction and shear stress increase at higher strain rates.

reduction as a function of strain rate. As strain rate increases, both the effective shear stress and velocity reduction increase. This is because as the effective shear stress increases, the displacement required to fully penetrate the target plate remains the same, so more work is required during penetration and velocity reduction increases. Goldsmith et al. [13] report a similar trend in velocity reduction when steel spheres were shot through steel and aluminum plates.

At the 850 and 1300 m/s impact velocities, the velocity reduction from the second plate penetration become more difficult to quantify and observe due to significant fragmentation. In a case with moderate to severe fragmentation, the penetration cannot be modelled as a cylindrical body, and while an average strain rate can still be calculated, the information is less meaningful because the projectile is no longer consolidated. Therefore, a more general approach discussed below is applied to study plate deformation mechanics.

3.2. Aluminum plate deformation

Fig. 5 shows the aluminum plates from both the front and back perspectives after penetration at 500 m/s. The fragmentation field after the first and second penetration event is almost non-existent so both penetration events can be simplified and analyzed as a cylindrical projectile penetrating a thin plate [11]. The first plate undergoes adiabatic shear plugging with the slightest degree of dishing apparent. For the second plate, some degree of adiabatic shear plugging occurs, however there is no separation of the projectile plug from the plate. The plug remaining attached to the plate is due to the propensity of thin targets to exhibit discing failure at lower impact velocities [11]. Discing failure occurs when shear fractures propagate parallel to the surface of the plate, allowing the plug to remain attached to the plate and fail through shear displacement instead of shear plugging. Failure through shear displacement instead of plugging results in a preferred direction of failure and the plate hinging open, which can partially be seen in Fig. 5 upper right corner. These asymmetrical failures often result in an increased resistance to failure which could also contribute towards more velocity reduction upon second plate penetration (Table 1).

Fig. 5 illustrates the increased radius of dishing failure observed upon second plate penetration. Specifically, there is a 20% increase in rupture size when the second plate is penetrated compared to the first. The size increase could be attributed to many different phenomena. It is possible that effects such as increased cross-sectional area of the projectile due to plastic deformation after penetration through the first plate (Fig. 3) will contribute to the rupture size increase as well as asymmetric shear banding. Also, penetration through the first plate induces stochastic motion into the projectile that could alter the projectile's flight path and add a degree of obliquity to the second plate impact, likely affecting the rupture size.

For the 850 m/s impact velocity shown in Fig. 6 there is a 34% increase in rupture size after penetration through the second plate. The first plate undergoes adiabatic shear plugging with no visible dishing [11], however projectile fragmentation does not allow for the second plate to be analyzed as a cylindrical projectile. Instead, the second plate penetration can be quantified through the cone angle of fragmentation [14]. Analysis of the video data reveals that the cone angle is 24° measured from the centerline of the catch chamber. The increase in rupture size may be a direct result of fragmentation spread not seen at lower velocities. The type of failure observed in the second plate is best described as petaling failure [15]. Cratering and pitting are observed around the peripheral of the hole in the second plate (Fig. 6) indicating that some fragmented debris does not contribute towards the second

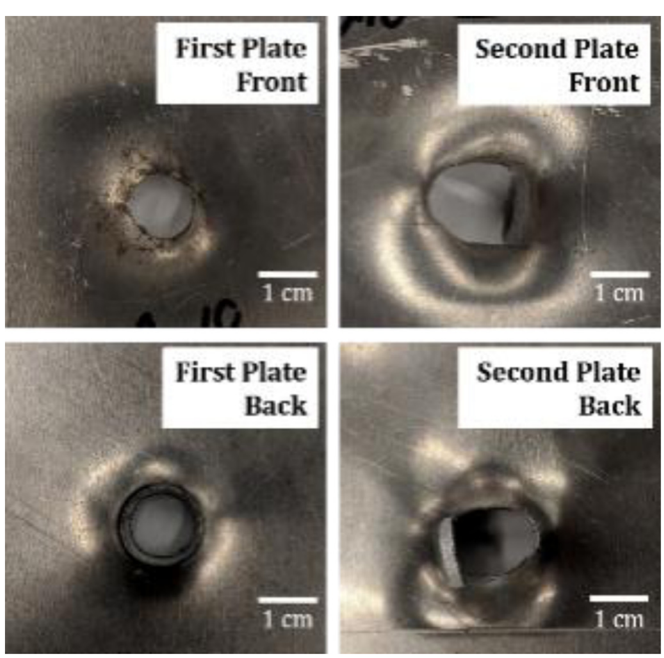

Fig. 5. Photographs of aluminum plates both front and back perspectives after penetration at impact velocity of 500 m/s. Note the scale bar in each image for size reference.

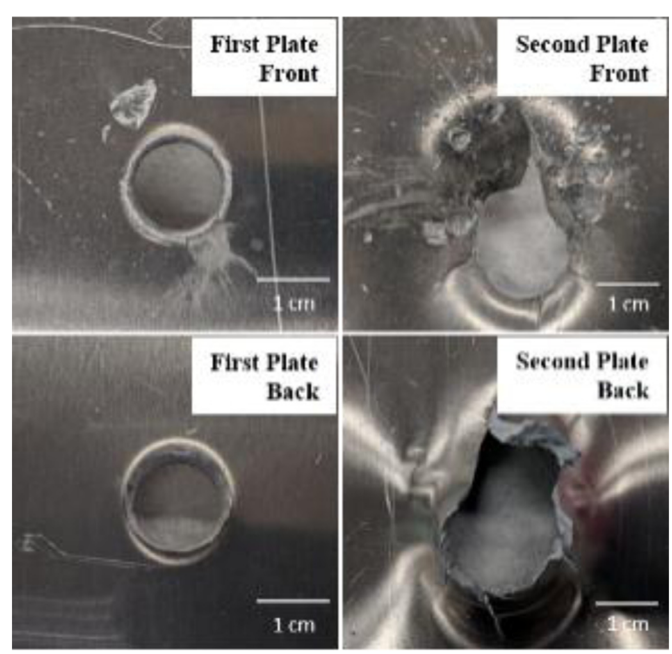

Fig. 6. Photographs of aluminum plates both front and back perspectives after penetration at 850 m/s. Note the scale bar in each image for size reference.

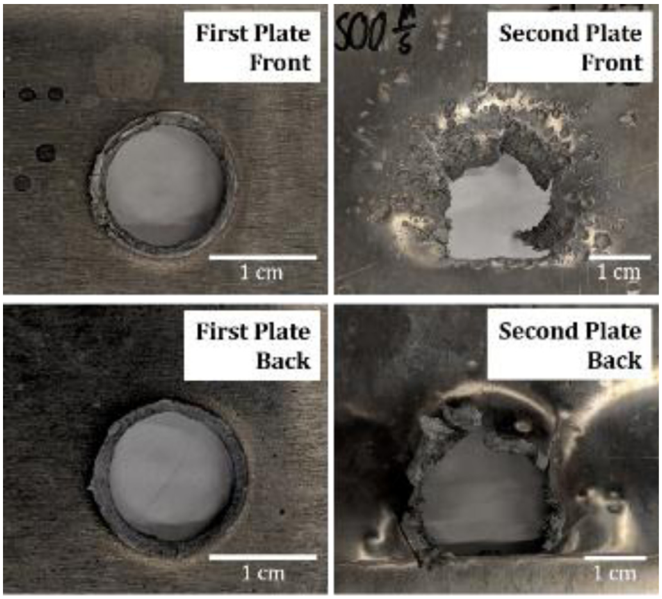

Fig. 7. Photographs of aluminum plates both front and back perspectives after penetration at 1300 m/s. Note the scale bar in each image for size reference.

Table 3
Measured and modelled radii for region affected by plate deflection. Measured deflections in the axial direction are also included. The average velocity between impact and residual velocities is v_{perf}.

Plate	v_{perf} *(m/s)*	Modelled Deflection Zone Radius (*cm*)	Measured Deflection Zone Radius (*cm*)	Measured Axial Deflection (*cm*)
First	439	3.9	1.1	0.15
First	772	2.2	0.79	0.08
First	1231	1.4	0.84	0.05
Second	259	6.6	1.98	0.43
Second	523	3.3	2.69	1.45
Second	961	1.8	3.48	1.52

penetration event and is instead lost through impact cratering.

For the 1300 m/s impact velocity shown in Fig. 7 there is a 45% increase in rupture size when the second plate is penetrated. Similar failure mechanisms are observed in the 850 m/s impact velocity, however the high impact velocity case exhibits more extreme behavior. Adiabatic shear plugging is still the main failure mode of the first plate and no dishing failure is observed. Fig. 7 also shows more extreme petaling failure. The cratering and pitting in the second plate are evidence of a greater density of impacts across the surface and imply fragmentation produced is finer and better dispersed than in the 850 m/s impact velocity case. Analysis of the video data reveals that the cone angle for fragmentation is 23° measured from the centerline of the catch chamber and the same cone angle produced from the 850 m/s impact velocity, indicating that an increased cone angle is not responsible for the increased rupture size. Instead, the increased density of the fragment cloud is likely the main factor affecting rupture size.

The size of the affected region surrounding the ruptured hole is investigated analytically and compared with experimental measurements, and results are summarized in Table 3. The impact velocity Mach number based on the elastic wave speed in the aluminum target plate may help explain the size of the effected region surrounding the ruptured hole. High velocity projectiles allow less time during the penetration event for elastic waves to travel away from the point of contact and therefore limit the amount of elastic deformation. A calculation of the affected region around the hole is made by estimating the distance an elastic wave will move through the plate over a time

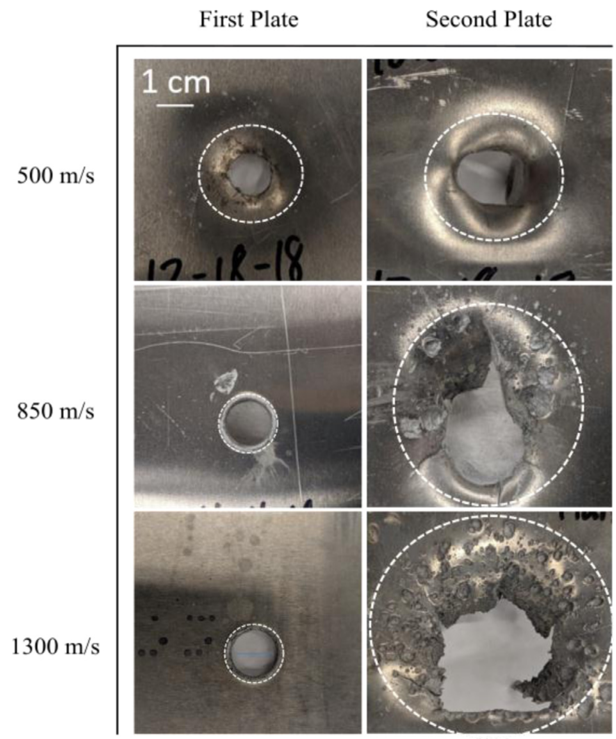

Fig. 8. Radius of plate region affected by deflection vs. impact velocity for first and second plates.

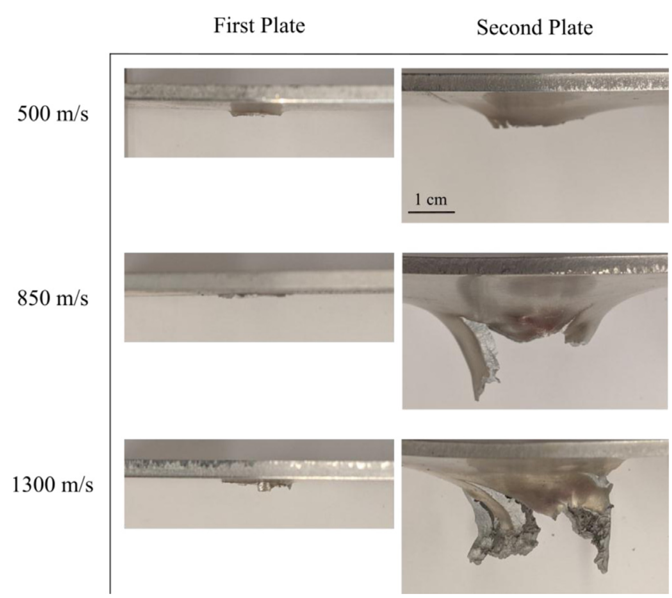

Fig. 9. Photographs of axial plate deflection as a function of impact velocity for first and second aluminium target plates.

scale comparable to the penetration event and modelled by $\delta t_{perf} = l/v_{perf}$, where l is the plate thickness and v_{perf} is the average velocity of the projectile during penetration so that $\delta t_{perf}$is the time between contact and complete penetration. The radius of the region showing deflection can then be estimated using Eq. (3) where $c_w$is the elastic wave speed in the plate.

$$r_{deflect} = \delta t_{perf} c_w \quad (3)$$

Order of magnitude estimates are made for these radii using the average of the impact and residual velocity for v_{perf} (Table 1) and a wave speed in the 6061-T6 aluminium plate of 5350 m/s [16] (Table 3).

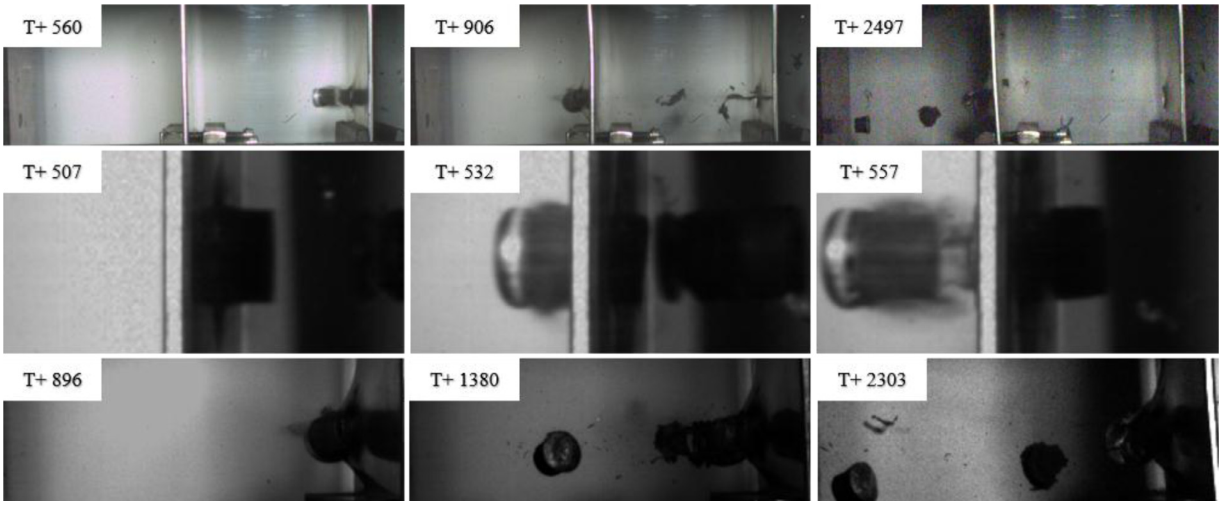

Fig. 10. Sequence of 500 m/s impact velocity images: time stamped still frames showing (top) full chamber view of projectile penetration through two plates, (middle) detailed view of penetration through first plate, (bottom) detailed view of penetration through second plate. Row 1 shows the projectile penetrating through the both plates with minimal fragmentation. Row 2 shows the projectile still fully intact during the first penetration event. Row 3 shows the projectile penetrating through the second plate and remaining intact.

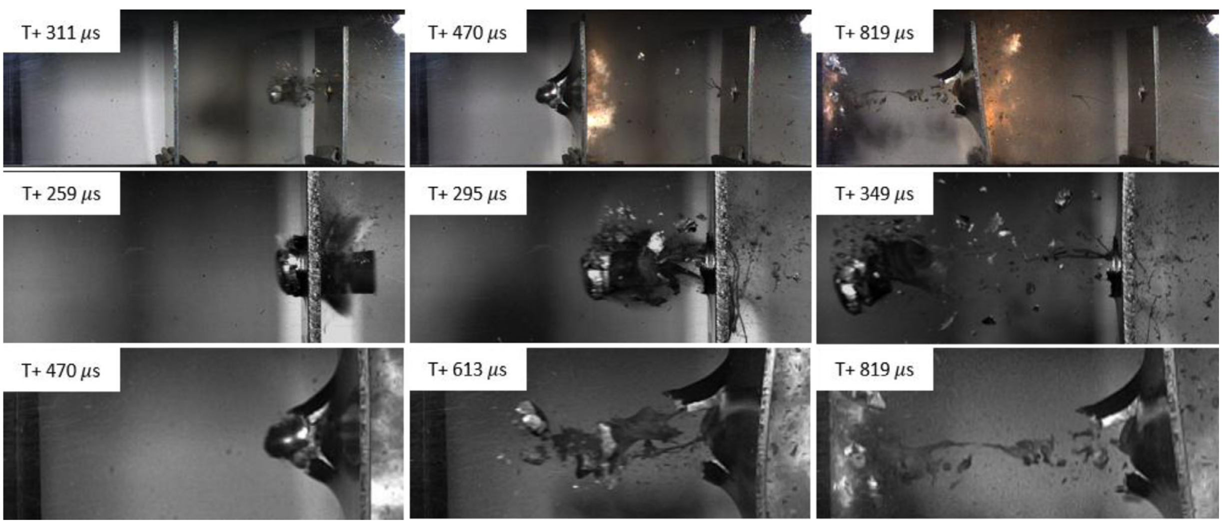

Fig. 11. Sequence of 850 m/s impact velocity images: time stamped still frames showing (top) full chamber view of projectile penetration through two plates, (middle) detailed view of penetration through first plate, (bottom) detailed view of penetration through second plate. Row 1 shows the projectile penetrating through both plates and anvil. Row 2 shows the projectile first penetration event. Row 3 shows the projectile penetrating through the second plate.

Because of the simplifications in the calculations presented above, model absolute values are less important than the trends reported in Table 3.

The trend between the measured deflection radii in the lowest and middle impact velocity experiments is similar to that of the simple model (Table 3) although the measurable radius of the experimental case is much smaller than the model. At higher impact velocity, the phenomenology of the penetration process appears to change to a simple plugging phenomena and no longer follows the trend based on elastic wave propagation. The model and experimental discrepancies are likely attributed to plastic yielding in the plates which reduces the magnitude of the forces resulting in deflection. As such, the comparison of the model and experimental data reveals that a transition in the mode of interaction between the plate and the projectile occurs between the middle and high impact velocity cases.

The deflections associated with the second plate impact and penetration are no longer expected to follow elastic wave trends because projectile fragmentation has taken place during the first plate impact. The fragmentation process not only breaks the projectile into smaller pieces but also disperses them so that the fragments hit the second plate in a more extended region than the footprint of the pristine projectile. According to the elastic wave model (Table 3), higher impact velocities should decrease deflection severity. The inverse trend is seen experimentally, indicating that fragmentation is a key function of the deflection severity.

Fig. 8 shows a visual representation of the deflection zone radius from Table 3. For the first plate, the 500 m/s impact velocity exhibits a small amount of dishing failure, whereas the 850 and 1300 m/s impact velocities only show deformation limited to the size of the plug displaced by the projectile. For the second plate, there is an increasing trend in deflection radius with impact velocity. The elastic wave propagation radius is modelled to a decrease as velocity increases, due to the projectile interacting with the target plate for less time, limiting the distance that elastic waves can travel. However, the elastic wave model assumes a uniform projectile penetrating the plate at all impact velocities. In both the 850 and 1300 m/s cases, fragmentation introduces a multitude of small bodies impacting the plate instead of a uniform projectile.

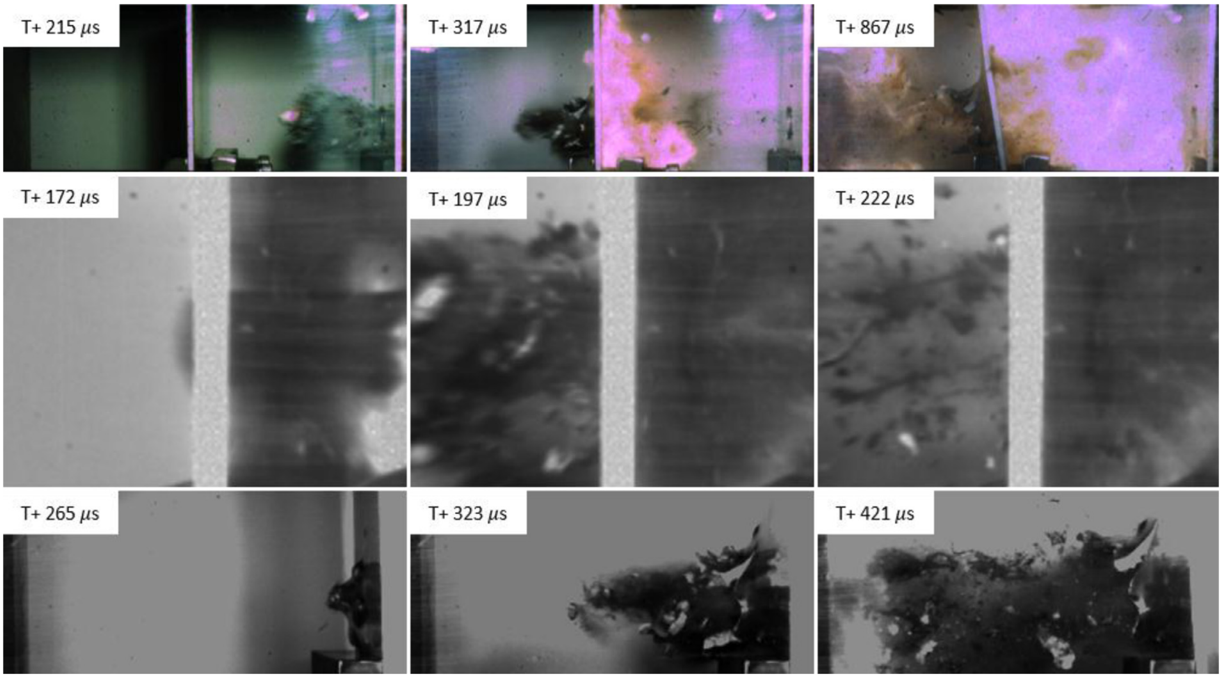

Fig. 12. Sequence of 1300 m/s impact velocity images: time stamped still frames showing (top) full chamber view of projectile penetration through two plates with purple coloring indicating flame spreading, (middle) detailed view of penetration through first plate, (bottom) detailed view of penetration through second plate. Row 1 shows the projectile penetrating through the two plates, fragmenting, and reacting. Row 2 shows the fragmentation directly after penetrating through the first plate. Row 3 shows the fragment cloud as it penetrates through the second plate (For interpretation of the references to color in this figure legend, the reader is referred to the web version of this article.).

Fig. 9 shows a side view of the plates to compare axially affected regions. The first plate shows the smallest degree of change, with the 500 m/s impact velocity showing minor dishing. Minor axial displacement in the first plate confirms that cylindrical projectile penetration mechanisms are largely unchanged across the impact velocities tested. The second plate deflections tend to get larger and more severe as impact velocity increases. Fragmentation is a key factor influencing this trend for the 850 and 1300 m/s velocities.

3.3. Visualization of penetration and impact

Fig. 10 shows a sequence of still frame images for the 500 m/s impact velocity that captures the entire chamber (top row), a detailed view of projectile penetration through the first plate (middle row), and a detailed view of the projectile penetration through the second plate (bottom row). For this case there is no flame spreading after any penetration or impact event and minimal observed reaction, and there is minimal fragmentation. The projectile remains completely intact throughout the entire event and only experiences plastic deformation in the form of mushrooming.

Fig. 11 corresponds to the 850 m/s impact velocity and shows a sequence of still frame images that capture the entire chamber, a detailed view of projectile penetration through the first plate, and a detailed view of the projectile penetration through the second plate (similar to Fig. 10). This is the lowest velocity tested that revealed reaction after impact such that a threshold velocity for reaction initiation exists between 500 and 850 m/s. While reaction is observed, the flame does not propagate through the chamber such that a flame spreading rate cannot be determined. Instead, the flame extinguishes prior to sustained propagation. The reaction produced during impact with the second plate is more significant than the reaction after impact with the steel anvil. It is interesting to note the small debris cloud produced after penetration through the first plate.

Fig. 12 corresponds to the 1300 m/s impact velocity and shows a sequence of still frame images similar to Figs. 10 and 11. Significant flame spreading is observed which can be tracked at the leading edge of the flame front as it travels to the front end of the chamber, similar to the projectile velocity analyses. The rate of flame spreading between the two plates is 500 m/s and the rate of flame spreading between the steel anvil and the second aluminum plate is 115 m/s, a reduction of 77%. It is interesting to observe significant flame spreading after penetration through the second plate that was not observed at the lower impact velocities. The observation of flame spreading indicates that the debris field contains particles that are small enough and carrying enough energy to react upon impact and produce flame. Intermetallic as well as oxidation reactions with the environment are both possible.

4. Conclusions

The strain rate of the system, and the ratio of wave speed to impact velocity, can be used to describe the different plate deformation mechanisms as the effective shear stress is highly dependent on strain rate. A threshold exists at which adiabatic shear plugging no longer occurs and instead shear deformation takes over and creates an asymmetric bending failure, largely due to plastic deformation occurring in the projectile. The increased overall velocity reduction between the first and second penetration plates can be explained due to the principles of work requiring more energy to account for the increased effective shear stress. These results show that impact velocity has a strong effect on projectile fragmentation and further influences reactivity as observed through flame spreading. The dramatic differences in plate morphology after penetration indicate impact velocity induces different penetration mechanics as the ballistic limit is notably exceeded.

Flame spreading is observed for intermetallic projectiles penetrating through aluminum target plates at impact velocities of 1300 and 850 m/s and appears to result from small particle debris within the fragmentation field. The rates of flame spread for the 1300 m/s case ranges from 500 down to 115 m/s, corresponding to the first and second penetration events. At the highest impact velocity, the fragmentation produced is finer and better dispersed. At the lowest impact velocity of 500 m/s, no flame spreading is observed and the debris field appears negligible with the projectile relatively intact even upon penetration of the second aluminum target plate. For this lower velocity impact case, the second plate appears to be plastically deformed with the puncture remaining hinged to the plate.

Declaration of Competing Interest

All authors declare none.

Acknowledgments

The authors MP, CC, CW, and KH are grateful for partial support from the Office of Naval Research (ONR). The authors also acknowledge Matsys, Inc. for fabricating all the projectiles used in this study.

Supplementary materials

Supplementary material associated with this article can be found, in the online version, at doi:10.1016/j.ijimpeng.2019.103427.

References

[1] Varma A. Form from fire. Sci American 2000;283(2):58–61.
[2] Fredrickson DC, Miller GJ. Intermetallic chemistry: new advances in humanity's age-old exploration of metals and alloys. Acc Chem Res 2018;51(2):213.
[3] Ames R.G.Vented chamber caloriemtry for impact-initiated energetic materials. Rd AIAA Aerosp Sci Meet Exhib2005:1–14.
[4] Ames R. Energy release characteristics of impact-initiated energetic materials. Multifunct Energ Mater MRS Proc 2006;896:1–10.
[5] Wang H, Zheng Y, Yu Q, Liu Z, Yu W. Impact-induced initiation and energy release behavior of reactive materials. J Appl Phys 2011;10:074904.
[6] Zhang XF, Shi AS, Qiao L, Zhang J, Zhang YG, Guan ZW. Experimental study on impact-initiated characters of multifunctional energetic structural materials. J Appl Phys 2013;113:083508.
[7] Lee RJ. Reactive materials studies. AIP Conf Proc. 845. 2006. p. 169–74.
[8] Hill KJ, Pantoya ML. Highly reactive pre-stressed aluminum under high velocity impact loading: processing for improved energy conversion. Adv Eng Mat 2019;1900492:1–7.
[9] Lambert J, Jonas G. Towards standardization in terminal ballistic testing: velocity representation. Aberdeen Proving Ground, MD: USA Balllistic Research Laboratories; 1976. Report No. 18521976.
[10] Elek PM, Jaramaz SS, Micković DM, Miloradović NM. Experimental and numerical investigation of perforation of thin steel plates by deformable steel penetrators. Thin-Walled Structures 2016;102:58–67.
[11] Woodward R. The interrelation of failure modes observed in the penetration of metallic targets. Internat J Impact Eng 1984;2:121–9.
[12] Gilat A, Clifton R. Pressure-shear waves in 6061-T6 aluminum and alpha-titanium. J Mech Phys Solids 1985;33:263–84.
[13] Golsdmith W, Finnegan S. Penetration and perforation processes in metal targets at and above ballistic velocities. Intern J Mech Sci 1971;13:843–66.
[14] Bratton R, Hill K, Magallanes J, Pantoya M. High velocity impact testing of intermetallic projectiles. Dyn Behav Mater Under Rev 2019.
[15] Corbett G, Reid S, Johnson W. Impact loading of plates and shells by free-flying projectiles: a review. Intern J Impact Eng 1996;18:141–230.
[16] Rae P, Trujillo C, Lovato M. The Young's modulus of 1018 steel and 6061-T6 aluminum measured from quasi-static to elastic precursor strain-rates Los Alamos National Laboratory; 2009. Report No. LA-UR-09-03627.